Effect of hyperbaric oxygen conditions on the ordering of interfacial water

Rolf E. Ypma, Gerald H. Pollack

Department of Bioengineering, University of Washington, Seattle, Washington USA

CORRESPONDING AUTHOR: Gerald H. Pollack – *ghp@u.washington.edu*

ABSTRACT

Hyperbaric oxygen (HBO_2) conditions are applied clinically to treat diverse conditions. There is a lack of a unifying consensus as to how HBO_2 acts effectively against a broad range of medical conditions, and numerous differing biological explanations have been offered. The possibility of a mechanism dependent on the extensive ordering of interfacial water has not yet been investigated. We examined the hypothesis that zones of ordered water, dubbed "exclusion zones" or "EZ," are expanded under hyperbaric oxygen conditions. Specifically, we tested whether there are significant quantitative differences in EZ size at steady state under high-pressure and/or high-oxygen conditions, compared to normal atmospheric conditions. Oxygen concentration and mechanical pressure were examined separately and in combination. Statistically significant increases in EZ size were seen at elevated air pressures and at high oxygen concentrations. These experimental results suggest the possibility of an ordered water-mediated mechanism of action for hyperbaric oxygen therapy.

INTRODUCTION

Hyperbaric oxygen (HBO_2) therapy is defined as a treatment in which a patient breathes 100% oxygen at a pressure above 1 atmosphere – generally 1.5 atmospheres or higher – that is applied within specially constructed pressure chambers [1]. HBO_2 is currently an FDA-approved treatment for a wide range of medical conditions. Primary targets are gas-based conditions such as decompression sickness, gas embolism and carbon monoxide poisoning [1]. However, HBO_2 therapy can also be applied to a range of wound-related indications, including necrotizing infections, gas gangrene, intracranial abscess, crush injuries and acute burns, as well as to conditions such as anemia and radiation injury. Various explanations exist for the mechanism through which HBO_2 acts upon different conditions. In the case of gas-based trauma, the elevated pressures of HBO_2 are thought to shrink trapped gas bubbles directly through increased pressure, as described by Boyle's law [2]. In wound treatments, increased atmospheric oxygen directly raises the partial pressure of oxygen in tissues, offsetting local hypoxic conditions that impede healing [2]. Elevated oxygen pressures also improve the oxygen-carrying efficiency of blood [1], thereby indirectly providing extra oxygen to tissues. Other studies have pointed to more complex mechanisms, such as the mobilization of stem cells [3]. Many mechanisms remain in doubt – for example, as a review of HBO_2 applications to traumatic brain injuries euphemistically observed: "the potential mechanism of action of HBOT in treating [brain injuries] has not been fully elucidated" [4]. While many of these theorized mechanisms may be valid, there appears to be no clear consensus regarding what makes HBO_2 function. It is suspected that rather than relying on a large, disparate collection of phenomena, the action of HBO_2 might be explained by a more fundamental systemic effect.

One candidate for this effect is the interfacial water surrounding proteins, membranes and many other biological surfaces. Interfacial water appears to be ordered, thereby excluding solutes; because of this excluding feature, the interfacial water zone has been dubbed the exclusion zone (EZ) [5]. Evidence suggests that water and other liquids form organized layers at interfaces [6]; water layering phenomena are observed in biological systems, and are significant factors affecting transport and other processes [7]. Recent work from this laboratory has characterized the prevalence, properties and behavior of these interfacial zones [5,8, 9,10].

Given that exclusion zones are ubiquitous features of biological systems, the question arose as to whether

KEYWORDS: hyperbaric oxygen, interfacial water

hyperbaric oxygen conditions might exert their influence by mediating changes in the EZ.

The hypothesized molecular structure for exclusion zones requires the splitting off of protons from bulk water [10,11], yielding a proton-poor exclusion zone with a higher ratio of oxygen to hydrogen than the bulk. Exclusion-zone formation and destruction are thought to be ongoing physical processes in interfacial water systems, where the EZ structure is simultaneously grown through a continuous input of incident infrared energy and destroyed by the influx of protons concentrated in the adjacent bulk. The exclusion zone is effectively in chemical equilibrium with the neighboring bulk water. This equilibrium should be governed by Le Chatelier's principle – that is, a change in conditions such as concentrations, system volume, or pressure will shift the equilibrium to compensate.

It was therefore hypothesized that hyperbaric oxygen conditions will increase the size of exclusion zones through two mechanisms: through increased pressure and through increased dissolved oxygen. A comprehensive review of exclusion-zone phenomena suggests that exclusion zones have a higher density than bulk water [5]. Therefore, increased pressure on the system should force the equilibrium more in favor of the exclusion zone by creating a drive to decrease volume, so the exclusion zone is expected to grow in size under high-pressure conditions. Furthermore, according to Henry's law, for a gas in equilibrium with a liquid, the amount of dissolved gas is proportional to the partial pressure: for oxygen at room temperature, $pO_2 = k_H \bullet [O_2]$, where $k_H = 769.2$ L atm mol^{-1}. An increased concentration of oxygen thus proportionally increases the abundance of oxygen dissolved in the water. Since EZs contain relatively more oxygen than bulk water, added oxygen may push the chemical equilibrium towards the exclusion zone.

We investigated these hypotheses, testing whether there are significant quantitative differences in exclusion zones at steady state under hyperbaric and/or high-oxygen oxygen conditions compared to normal atmospheric conditions.

METHODS AND MATERIALS

Exclusion zone measurements were achieved through a visualization protocol described in earlier work [8, 9], where Nafion samples were submerged in deionized water containing microspheres in suspension. The exclusion zone rapidly develops as a transparent interfacial zone on the order of several hundred micrometers extending from the Nafion surface, which can be visualized and quantified through visible-light microscopy.

An experimental pressure chamber for sample observation was constructed from aluminum (see Figure 1). A sample chamber region was machined from a 6-mm-thick aluminum plate, with a 16-mm *x* 20-mm hollow center. Threaded 1/8 inch steel tubing was attached to holes on two sides; tubing threads were sealed with silicone adhesive. Polymer tubing, sized to accept Luer-Lock syringe connectors, was inserted over the outer ends of the steel tubing. Above and below the sample chamber were two aluminum compression plates, with dimensions of 7.5 cm by 5.5 cm, which were drilled and threaded to accept a total of 10 steel bolts spaced evenly around the perimeter. Latex gaskets provided a seal between the central chamber walls and the tensioning plates, with 24 *x* 50 mm cover glass (VWR International) inserted over the top and bottom of the gaskets to cover the viewing window. Vacuum grease was applied to seal gaskets and chamber edges. For experiments, the chamber components were assembled and the plates tensioned to compress the gaskets, with one steel tube then used to introduce microsphere solutions to the sample chamber and the other used to modulate gas and/or pressure conditions. Total internal chamber and tubing volume was estimated at 5.0 mL by forcibly filling the entire apparatus with water, then forcibly draining the volume into a graduated cylinder. In experiments, 1.0 mL of volume was occupied by microsphere solution and Nafion tubing, leaving 4.0 mL of internal gas volume.

Microsphere suspensions were prepared with carboxylate-functionalized latex microspheres (Polysciences, Inc.) with a nominal diameter of 1 micron; actual diameter was 0.959 μm with SD 0.019 μm, as reported by the manufacturer. Concentrated microspheres were diluted at a rate of one drop (solids by volume 2.58%) to 5 mL of deionized water (Barnstead NANOpure Diamond), and vortexed gently to mix. Microsphere solutions were stored under refrigeration in 15 mL sterile polypropylene tubes (BD). The sample chamber contained a 1.5-cm length of Nafion tubing (Perma Pure, TT-070) with outer diameter 0.060 inches and wall thickness 0.006 inches (dry dimensions); a fresh piece of Nafion tubing was used for each experiment set. Using a 3-mL polypropylene syringe (BD), the sample chamber was loaded with 1 mL of microsphere solution, a quantity of solution sufficient to completely submerge the Nafion tubing without blocking the tube openings.

FIGURE 1. Pressure chamber

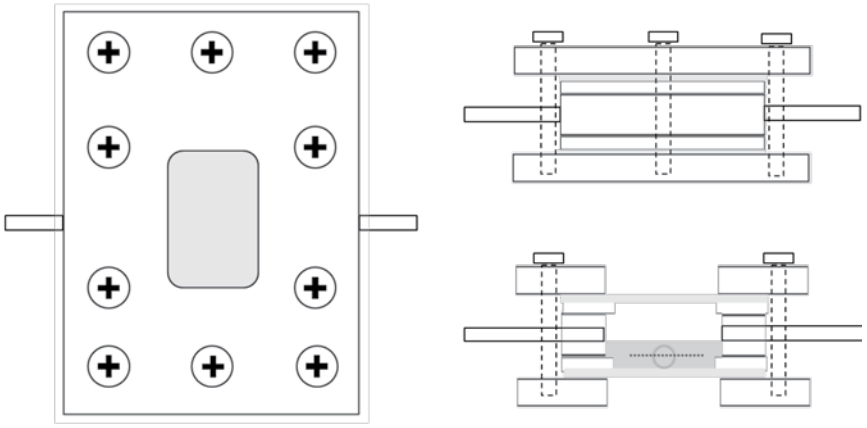

Construction of the pressure chamber, top view (left), side view (top right) and cutaway internal view (bottom right). Top view shows the layout of the central viewing window, gas input/outlet tubes, and compression screws; side view shows the layer arrangements of tensioning plates, glass covers (light blue), latex gaskets against glass covers, and the central chamber; cutaway view shows aqueous microsphere solution, Nafion tubing (central circle), the viewing path and the microscopy focal plane (horizontal dotted line). Top-view diagram is actual scale; side-view diagrams are vertically exaggerated to show features.

For air pressure experiments, the loading tube was clamped with hydrostat forceps after microsphere loading. A second 5-mL syringe was attached through a Luer Lock interface to the opposite tube to modulate pressure. This syringe was compressed to contract the chamber gas volume from 7.6 mL to 5.3 mL to achieve an approximate pressure of 1.43 atmospheres (calculations assume a relationship of $P_0 \cdot V_0 = P_1 \cdot V_1$, with temperature constant). This pressure level was confirmed by a pressure gauge attached to the loading tube. Syringe volume was modulated slowly, in order to not disturb the microsphere solution and disrupt the exclusion zone. The sample chamber was visualized through a Zeiss Axiovert 35 inverted microscope, using a Zeiss plan achromatic 5x objective lens. Images were captured with a CCD camera (Scion Corporation, CFW-1310C) with 1360- *x* 1024-pixel resolution, corresponding to a scale of 0.9 microns per pixel at the 5x objective magnification level.

For each air experiment set, the sample chamber was first allowed to equilibrate under normal atmospheric conditions for at least 30 minutes; equilibration was confirmed by observing that exclusion zone extent did not change visibly over a five-minute interval. Control measurements were captured of the final state of the equilibration period before experimental pressure conditions were applied. After pressurization, the chamber was again permitted to equilibrate for 30 minutes before data collection, although images of the initial states were also captured. Following data collection at 30 minutes, the syringe was carefully released and removed to restore pressure conditions to atmospheric, and the chamber was monitored for an additional 30 minutes to obtain a post-treatment control measurement.

To perform experiments with compressed nitrogen gas, an adapter was constructed to permit connection of a nitrogen cylinder's 1/4-inch gas inlet tube to the chamber's gas tubing via a Luer Lock interface. After microsphere loading, the loading tube was initially left unclamped while nitrogen was driven through the system at moderate pressure to ensure complete clearance of atmospheric gases. Later, the outflow tube was clamped and nitrogen pressure was increased to the desired level, as determined by a gauge on the nitrogen tank valve. Measurements of pressure levels, as well as chamber gas-tight seal integrity, were confirmed by a second gauge/valve assembly attached to the opposite side of the chamber. Finally, the gas inlet tube was clamped to seal the chamber before microscopy.

FIGURE 2. Image analysis

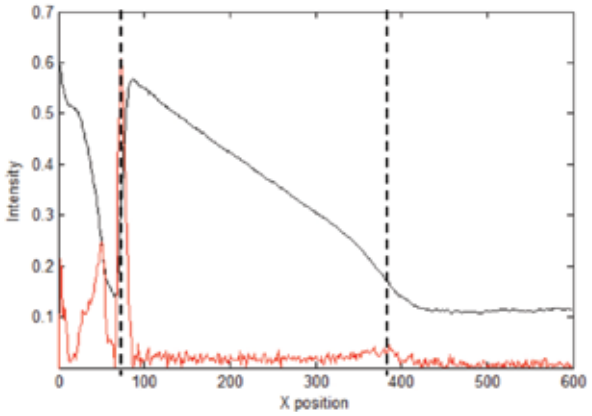

Representative plot of image processing analysis of microscopic images of exclusion zones. Black: normalized grayscale intensity. Red: intensity derivative, absolute value, normalized for visualization. Dashed lines represent the Nafion polymer boundary, at left, and the average EZ boundary across the region of interest, at right. These lines correspond to the pixel positions of the dark lines in Figure 3.

For experiments with compressed oxygen, a similar adapter was constructed to connect oxygen cylinders to the chamber tubing through a Luer Lock interface. With the outlet tube unclamped, oxygen was flowed at moderate pressure to clear atmospheric gases. The inlet and outlet were then clamped, and the outlet was momentarily released to normalize pressure to 1 atmosphere; positive chamber pressure prevented backflow of atmospheric gases during this procedure.

Image files were captured and examined with ImageJ, then cropped to show the region of interest, including the edge of the Nafion tube to beyond the farthest observed extent of the exclusion zone. A MATLAB image processing script was used to analyze images in a consistent manner, especially useful in cases where the exclusion zone was non-uniform across the viewing window. Briefly, the script converted images to double-precision grayscale, and then plotted the averaged intensity profile, and its derivative, in the direction perpendicular to the Nafion surface. The Nafion interface was easily located because the gel edge appeared dark due to refraction of the microscope light, whereas the exclusion zone appeared bright due to its transparency. In intensity plots (see Figure 2), this edge appeared as the steepest rise in intensity, corresponding to a local maximum in the derivative. Intensity then decreased linearly until the outer edge of the exclusion zone, where microspheres began to occlude light transfer and the edge appeared as an inflection point. The pixel distance between these two points corresponded to the average exclusion zone size, which was converted to the average EZ extent in microns by a factor of 0.9 μm per pixel, calculated from the microscope magnification and camera resolution. MATLAB script estimates were compared to manual image measurements to confirm consistency (see Figure 3), particularly in cases where EZs were irregular within the region of interest.

RESULTS AND DISCUSSION

Preliminary experiments were conducted to evaluate the null hypothesis that exclusion zones are unaffected by pressure or oxygen concentration. Experimental levels for air pressure were selected as 1 atmosphere for control measurements, 1.4 atmospheres to approximate the typical minimum used in hyperbaric therapy, and 0.6 atmospheres to represent a reduction of the same magnitude. Results are shown in Figures 4 and 5. The extent of exclusion zones was observed to generally increase with higher air pressure, vs. controls at atmospheric pressure. Exclusion zones were observed to contract in some cases under mild vacuum, although vacuum results were inconclusive overall.

Figure 4 shows mean exclusion zone size at each pressure condition. When viewed as independent samples, and assuming unequal variance, the difference between means was not found to be statistically significant with an unpaired t-test (p-values > 0.05). However, because data for each trial was first collected at equilibrium under control conditions, then collected again at a new equilibrium after air pressure was modulated, analysis of the EZ change is more meaningful and representative of the results – see Figure 5. Data based on before/after pairs necessitated a two-tailed paired t-test, which gave a p-value of 0.02314, indicating a statistical significance between control and 1.4 atm of air pressure with >95% confidence.

Because an increase in air pressure entails both an increase in the mechanical force acting on the fluid and an increase in oxygen partial pressure, further experiments were conducted to isolate the effects of these two variables. To isolate pressure effects, pure nitrogen gas was used as a substitute for atmospheric air. Although nitrogen is readily solubilized in water at approximately half the level of oxygen [12], nitrogen

FIGURE 3. EZ images

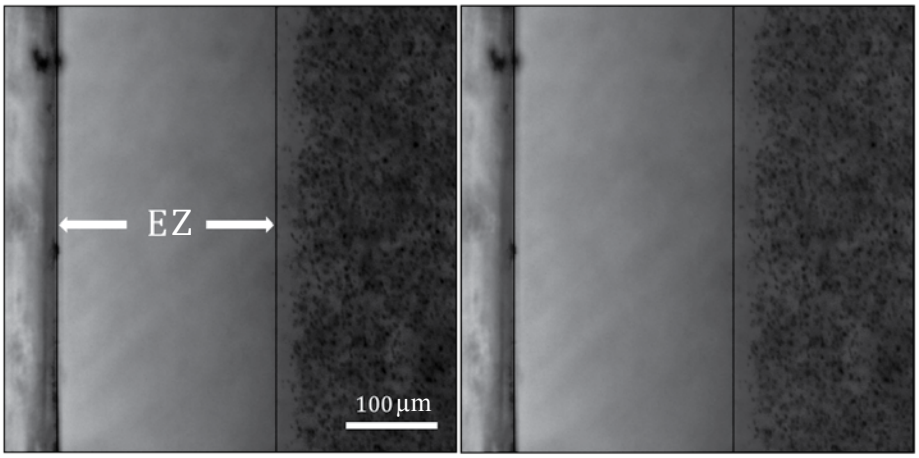

Representative microscopy image (grayscale), demonstrating agreement between image processing analysis and visual inspection. Black lines represent EZ boundary pixel positions as determined by image processing analysis, corresponding to the dashed lines in Figure 2. Image is from a trial with 95% oxygen at 1 atm pressure.

FIGURE 4. Mean EZ extent

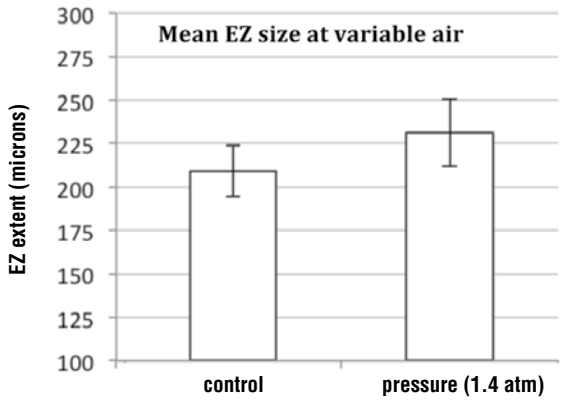

Mean EZ extent in microns at two air pressure conditions: control (1 atm) and mild positive pressure (1.4 atm). Error bars indicate standard error, with n = 10 for control, n = 7 at 1.4 atm.

FIGURE 5. Change in EZ extent

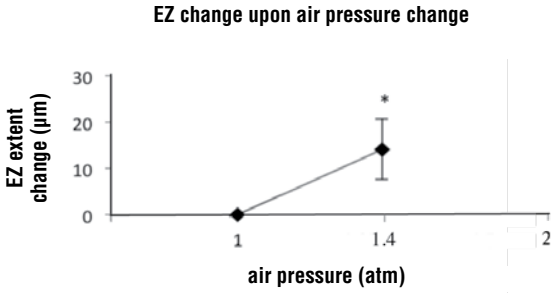

Change in EZ extent upon air pressure change, in microns. Error bars indicate standard error, with sample sizes as Figure 4; (*) indicates a statistical significant difference from control (p-value 0.02314).

was expected to be relatively inert compared to oxygen, and not interact chemically with the exclusion zone structure. For these experiments, pressures of 1, 1.41, 1.68 and 1.95 atmospheres were used to test for a correlation between pressure and exclusion zone extent. Representative images captured during trials at 1.41 atm and 1.95 atm absolute pressure are shown in Figure 6 and 7, respectively. Graphed results are shown in Figure 8. Early experiments showed promise of a positive linear correlation, but results were ultimately less conclusive due to inconsistent behavior. Figure 8 is a slightly unfortunate representation of these results – a single outlier at 1.4 atm is largely responsible for the large variance and poor linear correlation observed ($R^2 = 0.495$).

FIGURE 6

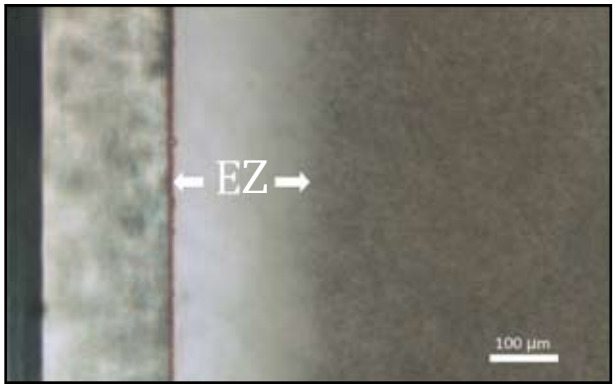

Figure 6 (left): Exclusion zone under 1.41 atm nitrogen pressure, after 30 minutes of equilibration, in unaltered color.

FIGURE 7

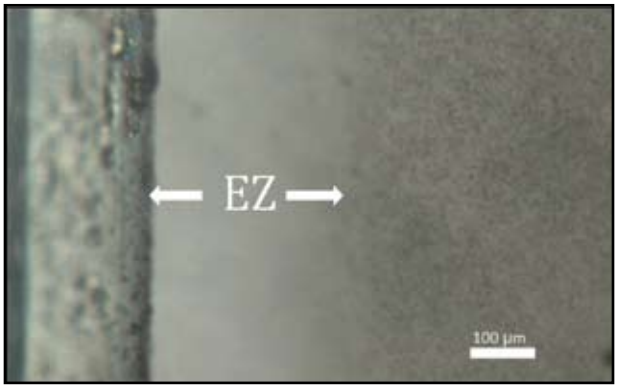

Figure 7 (right): Exclusion zone under 1.95 atm nitrogen pressure, after 30 minutes of equilibration, in unaltered color.

FIGURE 8. EZ extent at variable nitrogen pressure

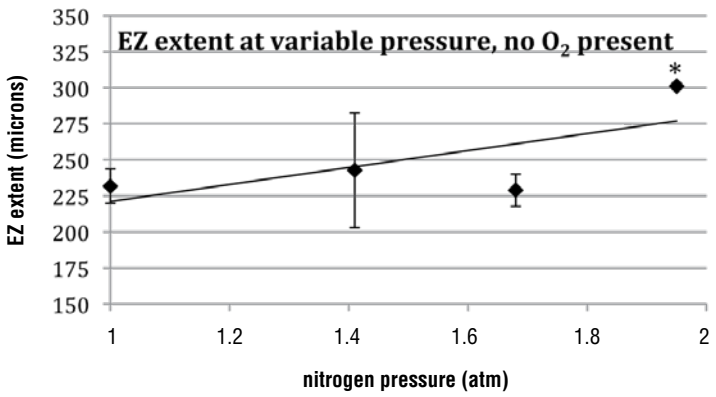

Mean EZ extent at different pressure conditions with a pure nitrogen gas atmosphere. Error bars indicate standard error, with n = 5 at 1 atm and n = 3 at other levels. (*) indicates a statistically significant difference from control with 95% confidence (p-value 0.00187). Linear correlation is poor (R2 = 0.495)

Although pre- and post-treatment measurements on the same samples would have been more satisfactory and would provide statistically stronger evidence, the necessity of flowing gas through the chamber to clear atmospheric gases proved problematic. Flowing gas was observed to create sufficient turbulence to disrupt any EZs present in the chamber, precluding meaningful before/after measurements. Measurements under experimental gas conditions and control conditions were thus conducted independently. This independence was reflected in statistical analysis through the use of unpaired t-tests, which ultimately showed no clear significant difference at 1.41 and 1.68 atmospheres ($p = 0.406$ and 0.436, respectively) but statistical significance at 1.95 atmospheres vs. control ($p = 0.00187$).

Therefore, there remains a distinct possibility that pressure alone is capable of causing EZ expansion, but the nature and extent of that effect is unclear. If this relationship is indeed real, the data suggest that the effect may be non-linear and evident only at higher pressures. Although the chamber constructed for these experiments could withstand pressures in excess of 2 atmospheres, during the experiments the chamber was never brought above 15-psi gauge pressure in the interest of safety and in compliance with the ASME Boiler and Pressure Vessel Code [13]. This limit was reasonable because this research was primarily concerned with the pressure ranges typically used in clinical HBO_2 therapy. Future experiments investigating pressure effects might use a more robust chamber design to probe a much greater range of pressures and observe more significant effects, although results at extreme pressures would be less relevant to clinical hyperbaric therapy.

The rationale for expecting an increase in EZ size with increasing pressure revolved around the hypothesis that, given that the EZ density is higher than that of bulk water, extra pressure on the system would

FIGURE 9. EZ extent at variable oxygen pressure

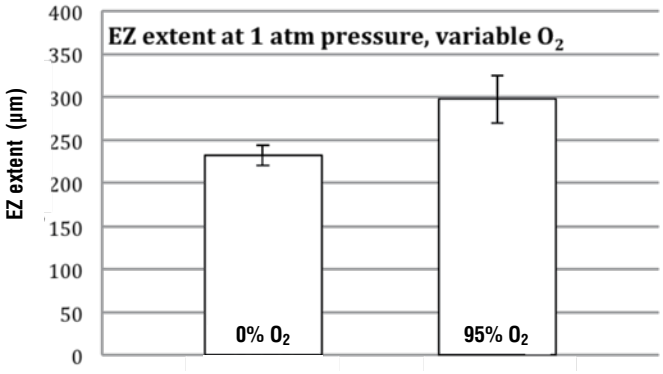

Mean EZ extent at varying levels of oxygen gas atmosphere. Error bars indicate standard error, with sample sizes n = 5 at 0% O_2 and n = 7 at 95% O_2. (*) indicates a statistical significant difference from control with 95% confidence (p-value 0.03193).

favor processes that contract the fluid volume, which should favor formation of the EZ phase. However, it is unknown whether Le Chatelier's principle of equilibria can be strictly applied to the EZ/bulk water system in this manner, as the system's dynamics remain poorly understood. Mechanical pressure may cause confounding effects – for example, one might envision a competing process in which increased pressure on the bulk tends to force concentrated protons from the bulk into the EZ, causing peripheral degradation of the EZ and size reduction. It appears that further study is necessary to reach a better understanding of pressure's true relationship with exclusion zones.

The nitrogen data did not adequately explain the behavior seen in the initial air pressure experiments. Therefore the final experiment set tested the effects of increasing oxygen concentration, with overall pressure fixed at 1 atmosphere, to test the hypothesis that addi-tional oxygen has a positive effect on EZs. Data from 100% nitrogen trials at 1 atmosphere was used to represent the 0% oxygen level, and independent trials were conducted with the chamber filled with 95% oxygen. As with nitrogen experiments, these trials were conducted in an independent manner because of the disruptive nature of gas flow through the chamber. Results are shown in Figure 9.

Figure 9 shows a statistically significant increase in mean exclusion zone size under 95% oxygen, with a p-value of 0.00187 in an unpaired, 1-tailed t-test assuming unequal variance. This result suggests that oxygen may be the primary factor in the observed EZ size increase seen with increased air pressure.

Several potential explanations exist for this phenomenon. The hypothesized structure for the exclusion zone is thought to contain a higher ratio of oxygen to hydrogen than bulk water. It was thus hypothesized that the availability of extra soluble oxygen would promote EZ formation. While this explanation is plausible, an exact chemical mechanism for incorporating dissolved oxygen species into the EZ structure is not immediately apparent. Such a mechanism might entail hydrolysis of water and/or the splitting of O_2, if O_2 is indeed the relevant soluble form.

A significant motivation behind this study was the idea that exclusion zones might be an explanatory factor in clinical hyperbaric oxygen therapy which appears efficacious for a wide variety of indications despite a mechanism still shrouded in mystery. It is thought that, given the abundance of both water and interfacial surfaces in living organisms, exclusion zones may be a highly prevalent phenomenon in biological systems. Exclusion zones might play a role in determining solute transport rates, ion gradients, viscosity and many other parameters within the highly interfacial architectures of biology. If the exclusion zone phenomenon does indeed play a significant role in biology, and oxygen levels have a significant effect on exclusion zones, then the elevated oxygen of HBO_2 might affect the body through an EZ mechanism.

Acknowledgments

Special thanks to Jeff Magula for invaluable assistance with the design and construction of the pressure chamber, and for assistance with handling the compressed-gas systems. Thanks also to Rushi Panchal for his help with the manuscript. Supported by NIH Transformative Grant# GM093842.

Conflict of interest

The authors have declared that no conflict of interest exists with this submission.

■

REFERENCES

1. Gesell LB (Chair and editor). Hyperbaric oxygen therapy indications. The Hyperbaric Oxygen Therapy Committee Report (12 ed.). Undersea and Hyperbaric Medical Society. 2008.

2. Tibbles PM, Edelsberg JS. Hyperbaric-oxygen therapy. N Engl J Med 1996, 334(25): 1642-1648.

3. Thom SR, Bhopale VM, Velazquez OC, Goldstein LJ, Thom LH, Buerk DG. Stem cell mobilization by hyperbaric oxygen. Am J Physiol Heart Circ Physiol 2006: 290 H1378-H1386.

4. McDonagh M, Helfand M, Carson S, Russman BS. Hyperbaric oxygen therapy for traumatic brain injury: a systematic review of the evidence. Arch Phys Med Rehabil 2004, 85: 1198-1204.

5. Pollack GH. The Fourth Phase of Water. Seattle, WA. Ebner & Sons. 2013.

6. Henniker JC. The depth of the surface zone of a liquid. Rev Mod Phys 1949, 21(2): 322-341.

7. Green K, Otori T. Direct measurements of membrane unstirred layers. J Physiol 1970, 207: 93-102.

8. Zheng J, Pollack GH. Long-range forces extending from polymer-gel surfaces. Phys Rev E Stat Nonlin Soft Matter Phys 2003, 68: 031408.

9. Zheng J, Chin W, Khijniak E, Khijniak Jr. E, Pollack GH. Surfaces and interfacial water: Evidence that hydrophilic surfaces have long-range impact. Adv. Colloid Interface Sci 2006, 127: 19–27.

10. Chai B, Yoo H, Pollack GH. Effect of radiant energy on near-surface water. J Phys Chem B 2009, 113: 13953-13958.

11. Klimov A, Pollack GH. Visualization of charge-carrier propagation in water. Langmuir 2007, 23: 11890-11895.

12. Pray HA, Schweickert CE, Minnich BH. Solubility of hydrogen, oxygen, nitrogen, and helium in water at elevated temperatures. Ind. Eng. Chem. 1952, 44(5): 1146-1151.

13. Boiler and Pressure Vessel Code. Section VIII – Rules for Construction of Pressure Vessels. American Society of Mechanical Engineers, 2007: U-1.

✦